

Submitted to Journal of Turbulence

Large-scale Flow Structures in a Planar Offset Attaching Jet with a Co-flowing Wall Jet

N. Gao*

School of Aeronautics and Astronautics, Dalian University of Technology, Dalian,
China

D. Ewing

Department of Mechanical Engineering, McMaster University,
Hamilton, Ontario, Canada L8S 4L7

* Corresponding author. Email:gaonan@dlut.edu.cn

Tel: +86(137)9519-0354

Fax:+86(411)8470-6202

Abstract

Conditional averaging techniques were used to examine the periodic motions that were observed in flows consisting of an offset planar jet and a co-flowing planar wall jet. The offset jet is one jet height (H_j) away from the wall and has a Reynolds number of approximately 40 000, based on H_j and flow-rate averaged velocity U_o ; for the co-flowing jets, different heights (i.e., $0.18H_j$ and $0.5H_j$) and velocities (i.e., $0.56U_o$ and $0.36U_o$) were considered. The flows had periodic motions with frequencies $fH_j/U_o = 0.28$ and 0.49 or $fH_c/U_o = 0.23$ and 0.25 , where H_c is the distance between the jets. The periodic motions were present in both the inner shear layer of the offset jet above the re-circulation region and the outer shear layer of the wall jet below the re-circulation region. The motions from the inner shear layer of the offset jet persisted in the shear layer that formed downstream of the re-circulating region. There were periodic motions in the outer shear layer of the offset jet particularly in the flow with the smaller wall jet. The relative contribution of the motions to the total fluctuations increased as the flow evolved downstream reaching a maximum approximately $4H_c$ downstream of the flow exit. The relative contribution of the periodic motions to the turbulent fluctuations was similar in the two flows but the periodic motions had a much larger impact on the near wall velocity and pressure fluctuations in the flow with the smaller wall jet due to the trajectory of the periodic structures, the distance of the periodic structures to the wall and the size of these structures.

Key words

offset attaching jet, co-flowing jets, large-scale structures

1 Introduction

Turbulent offset attaching planar jets, which are found in a variety of practical applications, have been characterized in a number of investigations [1–6]. The development of offset attaching jets are modified in some applications using a co-flowing wall jet below the offset jet. The addition of the wall jet provides mass that can be entrained into the offset jet and delays the interaction of the offset jet with the wall. The development of the co-flowing wall jet in these flows depends on a number of factors including the velocity of the wall jet [7–9]. Low velocity co-flowing wall jets separate from the wall at the exit and are quickly entrained into the offset jet, while higher velocity wall jets remain attached to the wall near the jet exit forming a re-circulation flow region between the co-flowing jets. The wall jet separates from the wall at a location below the re-circulating region downstream of the jet exit for moderate velocity wall jets but remains attached to the wall for higher velocity wall jets. The effect of the wall jet on the development of the offset jet appears to depend on the mass flow rate of the wall jet, while the change in the development of the wall jet and the formation of the recirculation region appears to depend more on the momentum flux of the wall jet [9].

The formation of the re-circulating flow region between the co-flowing jets (**sketched in Figure 1**) also appears to change the development of the large-scale structures in the flow by causing periodic motions that significantly increase the unsteady fluctuations normal to the wall in the inner shear layer of the offset jet and in the shear layer downstream of the re-circulating region [8–10]. The periodic motions appear to be associated with the re-circulating region between the co-flowing jets with a characteristic frequency that varies with the distance between the jets [9, 10]. Gao et al. [9] found that the effect of the periodic motions on the heat transfer rate to the co-flowing jets and the pressure fluctuations on the wall below the flow depended on the height of the wall jet in flows with a planar jet offset one jet height (H_j) from the wall. The effect was larger in a flow with a smaller wall jet. A comparison of the velocity spectra

and the two-point correlation between the pressure and velocity in the flows indicated that there was more interaction between the periodic motions in the wall jet and the wall below the re-circulating region for the flows with the smaller wall jet. There was also more interaction between motions in the shear layer formed downstream of the re-circulating region and the wall for the flow with the smaller wall jet, increasing the pressure fluctuations in this region [9]. The periodic motions also appeared to force the motions in the outer shear layer of the offset jet in the flows with the small wall jet though the effect of the forcing on the interaction of the periodic motions with the wall was unclear.

The objective of this investigation was to characterize the development of the periodic motions that formed in offset jets with higher velocity co-flowing wall jets considered in [9] using phase averaging techniques [11–13]. The phase averaged velocity throughout the field was computed based on a signal from the fluctuating wall pressure and this was then used to estimate the vorticity and pressure source terms associated with the periodic motions. The results do show the difference in the development of the periodic motions in the offset jets with different height co-flowing wall jets and clarify the role of the motions play in determining the near wall fluctuations. The experimental facility used for the measurements is reviewed here for completeness. The results of the analysis are then presented and discussed.

2 Experimental Methodologies

2.1 Facility

The measurements were performed using the flow facility shown in Figure 2, also used in Gao and Ewing [6, 9, 14]. **The coordinate system is shown in the figure.** The air flow from a **variable-frequency-drive-controlled** blower was split into an upper settling chamber (122 cm by 72.4 cm by 45.7 cm, **width by length by height**) leading

to an upper channel, and a lower settling chamber (81.3 cm by 40.6 cm by 22.9 cm) leading to a lower channel. The flow rate to each channel was adjusted using gate valves on the settling chamber inlets and the flows were conditioned in the settling chambers using layers of foam and perforated plates. The height of the upper channel, H_j , was 3.8 cm, and the distance from the wall to lower edge of the upper channel, H_s , was 3.8 cm. The heights of the lower channel, H'_j , were 0.7 cm ($0.18H_j$) or 1.9 cm ($0.5H_j$) for the flows with the smaller and larger wall jet, respectively, and bottom of the lower channel was flush with the wall in both cases. The length of the upper and the lower channels were 81 cm ($21.3H_j$) and 50.8 cm ($26.7H'_j$ when $H'_j=0.5H_j$), respectively. The width of the channels and the facility (into the page) was 74.3 cm ($19.6H_j$). The exits of both channels had machined square edges. The flow exiting the channels developed over a 1.8 m long plate mounted parallel to the channels. The facility included walls above the upper channel and the sides that extended approximately 100 cm ($26.3H_j$) above the bottom wall. The thickness of the boundary layers on the side walls were approximately $5H_j$ at $x/H_j = 12$ and $6H_j$ at $x/H_j = 16$. The profiles of the turbulent fluctuating velocity measured at $-5 \leq z/H_j \leq 5$ for the offset jet alone collapsed to within $\pm 3\%$ on the plane $x/H_j = 12$.

2.2 Wall pressure and velocity measurements

The fluctuating static pressure on the bottom wall was measured using 16 microphones (Panasonic WM-60B) that had flat responses for 20 Hz to 5000 Hz. The microphones were calibrated with a piston phone at 1000 Hz before the experiment. The microphones were then mounted directly into blind cavities drilled from the bottom of the wall and sensed the flow through a 1 mm-diameter, 5 mm-long pinhole drilled through the wall to the top of the cavity. There were 16 cavities at locations space $0.5H_j$ apart between $x/H_j = 0.5$ to 8 on a line that was 1.9 cm ($0.5H_j$) from the jet centerline.

The velocity measurements were performed using a cross hot-wire probe (sensors

$5\ \mu\text{m}$ in diameter, $1.5\ \text{mm}$ long) with an in-house anemometry system [16]. The hot-wire probe was calibrated in a round jet with a uniform exit velocity profile. The response curves were fit with fourth-order polynomials, and a modified cosine law [17]. The flow field was measured by moving the hot-wire probe on an overhead computer-controlled traverse that could be positioned with an accuracy less than $0.05\ \text{mm}$. Velocity measurements were performed on a grid directly above the microphone array ($z/H_j = -0.5$) with 16 evenly distributed stream-wise locations between $x/H_j = 0.5$ and 8. At each stream-wise location, measurements were performed at 20 vertical locations. The first measurement point was located $0.1H_j$ above the wall. The vertical distance between the adjacent measurement points was $0.1H_j$ near wall and expands by a factor of 1.03 at successive locations for $x/H_j = 0.5$. The expansion factor increased gradually in the stream-wise direction to 1.48 at $x/H_j = 8$ to cover the flow.

The velocity at each point was measured simultaneously with the wall pressure. The output signal from the anemometers and the microphones were sampled simultaneously using a 14-bit A/D board at a frequency of 2048 Hz for 75 seconds. The uncertainties in the **root-mean-square** velocity measurements due to sample size, evaluated following Brunn [17], was less than 3% for a 95% confidence interval. Rectification, examined following Tutu and Chevray [18], affected less than 2.5% of the data points at the inner half-width of the upper jet. The uncertainties for the fluctuating wall pressure due to the sample size was less than 4% for a 95% confidence interval. The spectra of the fluctuating velocities and wall pressure were computed from 150 blocks of data taken at each point in the flow field. The uncertainties in the magnitude of the spectra was estimated to be less than $\pm 8.2\%$ [19].

3 Results and Discussions

3.1 Time-averaged flow

Profiles of the mean velocity and the turbulent normal stresses measured near the channel exits for individual free jets were symmetric and fully developed [15]. The parameters of these two flows are summarized in Table 1. The flow rate averaged velocity (U_o) and momentum flux (\dot{M}) at the outlet of the offset jet were computed by integrating time averaged streamwise velocity (U) profile measured at $x/H_j = 0.05$ using a single hot-wire probe [9], shown in Figure 3(a). The profiles of the turbulence intensity (u'/U_o) measured at $x/H_j = 0.05$ are shown in Figure 3(b). The turbulence intensity (u'/U_o) was 0.041 at the center of the offset jet, and 0.019 and 0.031 in the wall jets with a height of $0.5H_j$ and $0.18H_j$, respectively.

The development of the large-scale structures was considered for the flows shown in Figure 4. The two wall jets have similar momentum fluxes but significantly different mass flow rates. The wall jets in both flows initially developed along the wall forming a re-circulation region between the offset jet and the wall jet. Surface oil flow visualization experiments [9] revealed that the wall jet in these two flows did separate from the wall near the end of the re-circulation region between the two jets but later re-attached forming a separation bubble under the wall jet. The streamline curvatures of the offset jet was more gradual in the flow with the larger wall jet that had the larger mass flow rate.

3.2 Spectral measurements

Typical spectra of the fluctuating velocities in flows and the fluctuating pressure on the wall below the flows are shown in Figure 5. The spectra had sharp peaks at a normalized frequency fH_j/U_o of 0.48 for the flow with the larger wall jet ($H'_j/H_j = 0.5$) and at

0.28 for flows with the smaller wall jet ($H'_j/H_j = 0.18$). The frequency of this peak did not change in the region considered here ($x/H_j \leq 8$) but the magnitude did decrease as the flows evolved downstream. The frequencies of these peaks were similar when they were normalized by the initial distance between the jets (fH_c/U_o of 0.23 and 0.25), suggesting the motions were associated with the presence of the **re-circulation** region between the jets.

3.3 Phase-averaged Reynolds stresses

The development of the periodic motions in the flows was examined with phase averaging techniques [11–13], using the wall pressure signal at x_R/H_j of 4 as the reference. The pressure signal was filtered using a fourth-order band pass Butterworth filter with a width of $0.02U_o/H_j$ centered around the frequency (f_R) corresponding to the sharp peak observed in the spectra for each flow ($f_R H_j/U_o$ of 0.28 and 0.49 in the flows with the small and large wall jets, respectively) as shown in Figure 5. This filter has been shown to have only a small effect on the phase of the filtered signal [12]. Examples of the original and the filtered signals are shown in Figure 6. The phases 0, π and 2π for each period were defined at the points when the filtered pressure signal became zero. The phase for each measurement point was then determined by

$$\begin{aligned}\phi &= \frac{t - t_{A,i}}{t_{B,i} - t_{A,i}}\pi, \quad t_{A,i} \leq t \leq t_{B,i} \\ \phi &= \frac{t - t_{B,i}}{t_{A,i+1} - t_{B,i}}\pi + \pi, \quad t_{B,i} \leq t \leq t_{A,i+1}.\end{aligned}\tag{1}$$

where $t_{A,i}$, $t_{B,i}$, and $t_{A,i+1}$ are the times corresponding to phase 0, π , and 2π for the i^{th} period. The phase of each 2π period was then divided into 60 equal intervals. All the data points that fell in the k^{th} interval of a period

were averaged using

$$\tilde{q}_k = \frac{1}{N} \sum_{j=1}^N q_{k,j}, \quad (2)$$

where q is the instantaneous quantity of interest (unfiltered fluctuating wall pressure or fluctuating velocity) and N is the total number of data points detected for each interval. There were typically 2500 points per interval.

The contribution of the periodic motions to the time averaged Reynolds stresses and the fluctuating wall pressure coefficient, determined by averaging the phase averaged quantities over one period [11, 13], are shown in Figure 7. The wall pressure fluctuations were much larger in the flow with the smaller wall jet and the results show that much of this difference was due to periodic fluctuations. The periodic motions initially contributed much of the vertical velocity fluctuations ($\bar{v^2}$) in the shear layer between the jets in both flows (Figure 7b and 7f). The periodic motions also contributed to the vertical velocity fluctuations in the outer shear layer of the offset jet downstream of the exit and to the vertical velocity fluctuations in the wall jet below the re-circulating region between the jets in the flow with the smaller wall jet. This did not appear to be the case for the flow with the larger wall jet. The periodic motions contributed to the stream-wise velocity fluctuations ($\bar{u^2}$) in the shear layer between the jets but the relative contribution was smaller than that for the vertical velocity fluctuations. There was evidence of periodic stream-wise fluctuations near the wall at x/H_j of 4 in the flow with the smaller wall jet (Figure 7e) that decreased as the flow evolved downstream from this point. These suggest an unsteady stream-wise accelerations near the wall in this region. The periodic motions do not appear to make a significant contribution to the stream-wise velocity fluctuations near the wall in the flow with the larger wall jet.

The average relative contribution of the periodic motions to the time averaged Reynolds stresses at different downstream positions can be characterized by integrating the quantities across the flow and computing their ratio; i.e., [11]

$$(\overline{\tilde{q}\tilde{s}}/\overline{q\tilde{s}})_m = \frac{\int_{0.05}^{Y_o} |\tilde{q}\tilde{s}| dy}{\int_{0.05}^{Y_o} |\overline{q\tilde{s}}| dy}, \quad (3)$$

where Y_o is the location where \overline{qs} was nearly zero. The results in Figure 8 show that the relative contribution of the periodic motions to the time averaged quantities increased as the flows evolved downstream reaching a maximum near the end of the re-circulating region between the jets in both flows. The contribution of the periodic motions then decreased as the flow and the periodic motions evolved downstream. The change in the contribution of the periodic motion were in better agreement when the downstream distance was characterized by the distance between the jets (H_c). The relative contributions of the periodic motions were similar in the two flows indicating the structures were not necessarily more dominant in the flow with the smaller wall jet though they would persist longer in this flow due to the larger separation distance between the jets.

3.4 Large-scale periodic motions

The periodic motions in the two flows can be characterized by the streamlines of the phase averaged velocity viewed from the reference frame moving with the motions [11]. The convection velocity of the periodic motions was determined by examining the rate of change in the time delay of the phase averaged measurements with downstream location, $U_c = \delta x / \delta \tau$, such as those shown in Figure 9. The convection velocity was $0.64U_o$ for the flow with the smaller wall jet and $0.76U_o$ for the flow with the larger wall jet. Convection velocities determined at different heights in the range $y/H_j \leq 1.6$ agreed. The results also agreed with the convection velocity determined from change in the phase of the cross spectra between the fluctuating wall pressure and the fluctuating velocity with downstream position at the reference frequency following [14]. The difference in the component of the mean convection velocity along the wall was due in part to the difference in the trajectory of the structures relative to the wall as discussed below.

Phase plots of the streamlines computed from the phase averaged velocity field at typical locations downstream of the re-circulating flow region between the co-flowing jets are shown in Figure 10. The streamlines computed from the phase averaged ve-

lacity field are viewed from a reference frame traveling at the convection velocity. The streamlines in both cases showed evidence of two sets of counter rotating motions. The lower row corresponded to the location of the shear layer that formed between the jets after they merged downstream of the re-circulating flow region, while the upper row corresponded to the location of the outer shear layer of the upper jet. The lower row of structures appeared to be closer to the wall in the flow with the smaller wall jet.

The periodic motions in the flow can also be characterized by examining the span-wise vorticity of the phase averaged velocity field estimated by

$$\tilde{\omega}_z = \frac{\partial(\tilde{v})}{\partial x} - \frac{\partial(\tilde{u})}{\partial y} \approx \frac{\Delta\tilde{v}}{\Delta x} - \frac{\Delta\tilde{u}}{\Delta y}, \quad (4)$$

where Δx was approximated by $\Delta x = -U_c\Delta t$. Here, U_c is the component of the convection velocity parallel to the wall. The derivative in y was computed by taking the finite difference of the phase averaged velocity. The uncertainty in the estimated span-wise vorticity of the phase averaged velocity field was estimated to be less than $\pm 8\%$ of the local value. The mean span-wise vorticity given by

$$\Omega_z = \frac{\partial V}{\partial x} - \frac{\partial U}{\partial y} \quad (5)$$

needs to be added to the span-wise vorticity from the phase averaged velocity field in order to properly reflect how the periodic motions contribute to the instantaneous vorticity. The first term ($\partial V / \partial x$) could not be accurately computed from the existing data though estimates suggest it is small. Thus, only the second term was used to estimate the local mean vorticity and this was added to the span-wise vorticity computed from the phase averaged velocity field. The phase plots of the vorticity result in Figure 11 for the flow with the larger wall jet showed a single row of structures that traveled along the shear layer that formed between the jets. The vorticity in the outer shear layer of the offset jet was primarily the contribution from the mean span-wise vorticity (or $-\partial U / \partial y$) because the contribution from the periodic motion was small relative to mean vorticity. This was not the case for the flow with the smaller wall jet indicating

that the periodic motions do affect the structures in the outer shear layer of the jet in this flow. The location of the vortices corresponded to the rotating motions in the streamlines in both cases.

Typical distributions of the phase averaged span-wise vorticity in the co-flowing jet flows at different points in the period are shown in Figure 12. The distributions of the vorticity in both flows showed a row of periodic structures in both the inner shear layer of the offset jet above the re-circulation region and the outer shear layer of the wall jet below the re-circulation region. The motions from the inner shear layer of the offset jet persisted in the shear layer formed after the jets merged downstream of the re-circulating region while the structures from the wall jet did not appear to persist. The vorticity of the structures in the shear layer downstream of the recirculation region have the same sign as the mean vorticity in this region. The structures traveled approximately parallel to the wall in the flow with the larger wall jet, but traveled toward the wall in the flow with the smaller wall jet. The structures were also closer to the wall near the mean re-attachment location in the flow with the smaller wall jet. The structures followed the shear layer between the jets and thus much of the difference in the trajectory in the structures is due to the difference in the trajectory of the offset jet, which is affected by the mass flow rate of the wall jet. There were periodic motions in the outer shear layer of the offset jet in the flow with the smaller wall jet that grew as the flow evolve downstream and persisted beyond the near field region. The structures in the outer shear layer evolved approximately in phase with the motions formed in the inner shear layer of offset jet. It is thought that the periodic motions occur in the outer shear layer of the offset jet in this flow because the periodic frequency associated with the recirculation region better matches the natural frequency of the motions in the outer shear layer.

3.5 Wall pressure fluctuations

The role of the periodic motions in determining the periodic pressure fluctuations was examined using the Poisson equation given by the following equation in the Einstein convention [20]

$$\frac{\nabla^2 p}{\rho} = -2 \frac{\partial U_i}{\partial x_j} \frac{\partial u_j}{\partial x_i} - \frac{\partial^2}{\partial x_i \partial x_j} (u_i u_j - \bar{u}_i \bar{u}_j), \quad (6)$$

where U_i and u_i ($i=1,2,3$) represent the three components of the mean and the fluctuating velocities, respectively. The first or rapid term is linear in the fluctuations, so the phase averaged velocity fluctuations will contribute to the phase averaged pressure fluctuations through this term. The contribution of three components of the rapid term computed from the phase averaged velocity field (based on the reference pressure at x_R/H_j of 4) are shown in Figure 13. Derivatives of the phase averaged velocity field in the stream-wise direction were estimated using Taylor's hypothesis. The derivatives in the y direction were again estimated using a finite difference approach. The uncertainty in the results was estimated to be less than $\pm 8\%$. The distributions of the pressure source terms show that $-2(\partial U / \partial y)(\partial \tilde{v} / \partial x)$ was the largest of the linear source terms considered here, particularly in the region near the wall. The mean velocity gradient in the fourth term $-2(\partial V / \partial x)(\partial \tilde{u} / \partial y)$ could not be reliably computed but estimates suggest this term was modest over much of the flow.

The change in the distribution of the fluctuating pressure source term $-2(\partial U / \partial y)(\partial \tilde{v} / \partial x)$ with phase in the co-flowing jets are shown in Figure 14. There were regions where the pressure source terms were positive or negative that traveled along the shear layer between the jets downstream of the recirculation region. The positive regions corresponded to the regions of large negative vorticity or the vortical structures that traveled along this shear layer in Figure 12. The negative regions corresponded to the region between these vorticities where a positive vorticity from the phase averaged field reduced the contribution from the mean vorticity. The regions were more compact in the flow with the larger wall jet but had a larger local maximum or minimum consistent with

the more compact structures observed in this flow. The sources traveled parallel to the wall in the flow with the larger wall jet but traveled toward the wall for the flow with the smaller wall jet similar to the periodic structures. There were also regions of positive and negative source terms in the outer shear layer of the jets. The positive terms corresponded to the regions of positive vorticity in this shear layer in Figure 12 and were more prominent in the flow with the smaller wall jet. The positive source terms will result in a negative local fluctuating pressure at the center of the vorticities in both shear layers, as expected.

The effect of fluctuating pressure source terms in the flow on the pressure fluctuations on the wall can be determined by solving the Poisson equation for the pressure. In this case, the source terms were multiplied by $-1/4\pi r$ where r is the distance from each point in the flow (x, y, z) to the location of interest (x_o, y_o, z_o) ; *i.e.* $r^2 = (x - x_o)^2 + (y - y_o)^2 + (z - z_o)^2$. The results can then be integrated over the field to determine the effect of the source terms throughout the flow on the local fluctuating pressure [21, 22]. The contribution of the pressure sources determined from the phase averaged velocity field to fluctuating pressure on the wall at $x_o/H_j = 4$ and $z_o = 0$ are shown in Figure 15. The results here are for points in the flow on the same plane ($z = z_o$) at the point of interest. The results showed that the contribution from the individual source terms in the shear layer to the wall pressure fluctuations were not small, but they alternated and tended to cancel. A three dimensional integration of the source terms over the region shown was made assuming that the structures were two-dimensional (which was a reasonable first approximation in these flows). The results indicated that the sources in the near wall region $y/H_j \leq 0.1$ made much of the contribution to the wall pressure fluctuations in both flows. The effect of the alternating source terms from the periodic motions in the shear layers, though not small tended to cancel each other.

3.6 Discussion

The estimates of the pressure source terms associated with the periodic motions in Figure 15 suggest that the difference in the wall pressure fluctuations observed downstream of the recirculation region in the two flows considered here is due to differences in the unsteady motions induced near the wall by the periodic motions in the shear layer between the jets. The induced motions appeared larger in the flow with the smaller height wall jet because the periodic motions in this flow are larger and travel closer to the wall (Figures 11 and 12). There were differences in the periodic motions in the two flows; the size of motions were larger in the flow with the smaller height wall jet as noted, the local vorticity associated with motions was smaller in the flow with the smaller height wall jet (Figure 12), and the estimated pressure source terms (Figure 14) associated with the periodic motions were smaller for the flow with the smaller height wall jet. Much of the differences appeared related to the size of the splitter plate (H_c). The results are in better agreement when they are scaled using the size of the splitter plate (H_c) rather than the jet height (H_j) and compared at the same downstream position relative to the splitter plate (x/H_c) similar to the results for the contribution of the motions to the turbulent Reynolds stresses (cf Figure 8). There was also evidence of periodic motions in the outer shear layer of the offset jet with the smaller height wall jet but they did not appear have a significant effect on the development of the flow in the region considered here.

The trajectory of the periodic motions in the two flows differed. The periodic motions formed in the inner shear layer of the offset jet follow the shear layer that forms between the jets when they merged downstream of the recirculation regions. The center of the periodic motions reach the cen-

ter of the splitter plate between the jets much more quickly in the flow with the smaller wall jet (more so in terms in x/H_c) and moved beyond this point to approach the wall (Figure 12). Thus, the difference in the interaction of the structures with the wall is more than that would be anticipated by simply allowing for the larger structures and smaller distance from the wall to the center of the splitter plate in the flow with the smaller height wall jet. The trajectory of the offset jets toward the wall in these flows with a co-flowing wall jet are affected by the mass flow rate of the wall jet [9], and the mass flow rate of the smaller height wall jet considered here is less than that of the larger height wall jet. The pressure fluctuations below flows with higher velocity smaller height wall jets are substantially larger than those for the flow with the larger height wall jet (even for similar mass flow rate wall jets) [9]. When the conditional averaging approach was applied to the measurements of the fluctuating pressure below the flows with the higher velocity small height wall jets, it was found that the periodic motions are responsible for most of the difference as shown in Figure 16. Increasing the mass flow rate or velocity of the wall jet increases the wall pressure fluctuations below the recirculating flow region between the jets, but decreases the wall pressure fluctuations and the contribution from the periodic motions downstream of the recirculation region. There does not appear to be a mean separation bubble below the high flow rate wall jets [9] suggesting this did not play a significant role in the wall pressure fluctuations although the presence of the recirculation region may affect the initial interaction of the structures with the wall. Projecting the decay in the contribution of the periodic motions in Figure 16 back toward the recirculation region suggests an earlier interaction between the structures and the wall in the flows with the higher velocity small height wall jets. The difference between the results for the different flow rate small height wall jets are much less than the

difference between the results for large and small height wall jets. Thus, the results indicate that the height of the wall jet, which affects both the height of the shear layer downstream of the recirculation flow region and the size of the structures, is a larger factor.

4 Conclusions

Conditional averaging techniques were used to examine the periodic motions that occurred in flows with a planar offset jets and a co-flowing wall jet in cases where the wall jet initially developed along the wall causing a re-circulation region between the jets. The analysis was performed for jets initially offset one jet height above the nearby wall with co-flowing wall jets with heights of 0.5 and 0.18 times this offset height. The wall jets in the two flows have similar momentum fluxes but different mass flow rates. Both wall jets initially travel parallel to the wall and separate from the wall at a location downstream of the jet exit, forming a re-circulation region between the two jets. The phase averaged flow fields in both cases showed that periodic motions developed in the inner shear layer of the offset jet above the re-circulation region between the two jets and traveled along the shear layer formed between the two jets downstream of the re-circulation region.

The contribution of the periodic motions to the Reynolds stresses initially increased as the motions developed downstream before decreasing downstream of the re-circulation region. The distance to the maximum in the relative contribution of the periodic motions increased with the separation distance between the co-flowing jets and thus persisted further downstream in the flow with the smaller wall jet. The relative contribution of the periodic motions to the Reynolds averaged turbulent stresses in the flows were similar when the downstream distance was normalized by the initial distance between the jets.

The effect of the periodic motions on the pressure fluctuations on the wall and the

flow near the wall differed in the two geometries with much larger near wall fluctuations in the flow with the smaller wall jet. Much of the differences in the effect of the structures on the near wall velocity and pressure fluctuations appears to be caused by differences in the proximity of the structures to the wall. The distance from the wall to the outer shear layer of the wall jet below the re-circulation region and the shear layer formed downstream of the re-circulation region varied with the wall jet height and thus the structures formed in the flow with the smaller wall jet were much closer to the wall. The size of the structures also appears to vary with the initial distance between the jets and thus is larger in the flow with the smaller wall jet. All these factors would act to increase the interaction between the structures and the wall though the proximity of the structures is the larger factor for the cases considered here.

Acknowledgment

This work was funded by the Natural Sciences and Engineering Research Council of Canada. The authors wish to acknowledge Ms. L. C. Ofiara for her assistance in preparing the manuscript.

References

- [1] R. Sawyer, *Two-dimensional reattachment jet flows including the effect of curvature on entrainment*, J. Fluid Mech. 17 (1963), pp.481-498.
- [2] C. Bourque, *Reattachment of a two-dimensional jet to an adjacent flat plate*, in *Advances in Fluidics* F. Brown eds., ASME Press, New York, 1967, pp. 192-204.
- [3] T. Lund, *Augmented thrust and mass flow associated with two-dimensional jet reattachment*, AIAA J. 24 (1986), pp.1964-1970.
- [4] J. R. R. Pelfrey and J. A. Liburdy, *Mean flow characteristics of a turbulent offset jet*, J. Fluids Engr. 108 (1986), pp.82-88.
- [5] A. Nasr and J. C. S. Lai, *Comparison of flow characteristics in the near field of two parallel plane jets and an offset plane jet*, Phys. Fluids 9 (1997), pp. 2919-2931.
- [6] N. Gao and D. Ewing, *Experimental investigation of planar offset attaching jets with small offset distances*, Exp. Fluids 42 (2007), pp.941-954.
- [7] N. Gao, D. Ewing and J.W. Naughton, *Measurements of wall shear stress of an offset attaching planar jet with co-flow*, AIAA paper 2006-0646.
- [8] Z. Li, W. Huai, and Z. Yang, *Interaction between wall jet and offset jet with different velocity and offset ratio*, Procedia Engr. 28 (2012) pp. 49 - 54.
- [9] N. Gao, C.Y. Ching, D. Ewing and J.W. Naughton, *Heat transfer and flow measurements of a planar offset attaching jet with a co-flowing jet*, Int. J. Heat Mass Transfer 78 (2014), pp.721 - 731.
- [10] N. Gao and D. Ewing, *Investigation of the large-scale flow structures in dual planar attaching jets*, AIAA paper 2006-0313.

- [11] M. Matsumura and R. Antonia, *Momentum and heat transport in the turbulent intermediate wake of a circular cylinder*, J. Fluid Mech. 250 (1993), pp.651-668.
- [12] Y. Zhou and M. Yiu, *Flow structure, momentum and heat transport in a two-tandem- cylinder wake*, J. Fluid Mech. 548 (2006), pp.17-48.
- [13] J. Hu and Y. Zhou, *Flow structure behind two staggered circular cylinders. part 2. heat and momentum transport*, J. Fluid Mech. 607 (2008), pp.81-107.
- [14] N. Gao and D. Ewing, *On the phase velocities of the motions in an offset attaching planar jet*. J. Turbulence 9 (2008) No.27.
- [15] N. Gao, *Offset attaching planar jets with and without a co-flowing jet*, Ph.D. thesis, McMaster University, Canada, 2006.
- [16] S. Woodward et al., *Anemometer system review*, 6th International Symposium on Hot-Wire Anemometry, Jan. 8-10, 2001, Melbourne, Australia.
- [17] H. Bruun, *Hot-wire Anemometry* (Oxford: Oxford University Press), 1995.
- [18] N. Tutu and R. Chevray, *Cross-wire anemometry in high intensity turbulence*, J. Fluid Mech. 71 (1975), pp.785-800.
- [19] J.S. Bendat and A.G. Piersol, *Engineering Applications of Correlation and Spectral Analysis* (New York: John Wiley and Sons), 1993.
- [20] S. Pope, *Turbulent Flows*, (Cambridge: Cambridge Press), 2000.
- [21] G. Corcos, *The structure of the turbulent pressure field in boundary-layer flows*, J. Fluid Mech. 18 (1964), pp. 353-378.
- [22] A. Naguib and M. Koochesfahani, *On wall-pressure sources associated with the unsteady separation in a vortex-ring/wall interaction*, Phys. Fluids 16 (2004), pp.2613-2622.

Table 1: Summary of flow parameters of offset jet and co-flowing jets

H'_j/H_j	$U'_o H'_j/\nu$	$U_o H_j/\nu$	U'_o/U_o	$\dot{M}' \text{ [kg/s}^2\text{]}$	$\dot{M} \text{ [kg/s}^2\text{]}$
0.18	4420	42140	0.56	0.91	14.8
0.5	7550	41000	0.36	1.1	14.9

Figure list:

Figure 1: Schematics of the planar offset attaching jet with a co-flowing wall jet.

Figure 2: Schematics of the experimental facility and flow measurements.

Figure 3: Profiles of the (a) time averaged stream-wise velocity and (b) turbulence intensity measured at $x/H_j = 0.05$ using a single hot-wire probe for planar offset jets with an offset distance H_s of H_j and co-flowing jets with heights H'_j of $\square 0.5H_j$ and $\bullet 0.18H_j$.

Figure 4: Vectors and streamlines of the mean velocity in planar offset jets with an offset distance H_s of H_j and co-flowing jets with heights H'_j of (a) $0.5H_j$ and (b) $0.18H_j$. The vertical arrow denotes the mean reattachment location.

Figure 5: Spectra of the stream-wise (F_{uu}) and vertical (F_{vv}) fluctuating velocities, and the fluctuating wall pressure (F_{pp}) at $x/H_j = 3$ and $y/H_j = 0.75$ for co-flowing jets with (a) $H'_j/H_j = 0.5$ and $U'_o/U_o = 0.36$ and (b) $H'_j/H_j = 0.18$, $U'_o/U_o = 0.56$.

Figure 6: Transient of the reference pressure at $x_R/H_j = 4$ and u and v at (a) $x/H_j = 4$ and $y/H_j = 1$ for the flow with $H'_j/H_j = 0.5$ and $U'_o/U_o = 0.36$ and (b) $x/H_j = 4$ and $y/H_j = 0.6$ for the jets with $H'_j/H_j = 0.18$ and $U'_o/U_o = 0.56$. The dash lines are the filtered signals.

Figure 7: Profiles of \circ the Reynolds averaged fluctuating velocities, shear stress, and pressure (e.g., \overline{uv}) and \bullet the phase averaged (mean subtracted) velocities, shear stress, and pressure averaged over one period (e.g., $\overline{\tilde{u}\tilde{v}}$) for (a-d) the co-flowing jets with $H'_j/H_j = 0.5$ and $U'_o/U_o = 0.36$ when $x_R/H_j = 4$ and $f_R H_j/U_o = 0.49$ and (e-h) the co-flowing jets with $H'_j/H_j = 0.18$ and $U'_o/U_o = 0.56$ when $x_R/H_j = 4$ and $f_R H_j/U_o = 0.28$.

Figure 8: Change of the contribution of the motions with the phase averaging frequency f_R to the time averaged Reynolds stresses with downstream positions (a) relative to the offset distance of the outer jet and (b) the initial distance between the jets for \circ the co-flowing jets with $H'_j/H_j = 0.5$ and $U'_o/U_o = 0.36$, and for \bullet the co-flowing jets with $H'_j/H_j = 0.18$ and $U'_o/U_o = 0.56$.

Figure 9: Contours of \tilde{v}/U_o at different time delays ($\tau = \phi/2\pi f_R$) at $y/H_j = 0.65$ (a) in the co-flowing jets with $H'_j/H_j = 0.5$ and $U'_o/U_o = 0.36$ when $x_R/H_j = 4$ and $f_R H_j/U_o = 0.49$ and (b) in the co-flowing jets with $H'_j/H_j = 0.18$ and $U'_o/U_o = 0.56$ when $x_R/H_j = 4$ and $f_R H_j/U_o = 0.28$. The cutoff level is ± 0.02 , the contour interval is 0.02.

Figure 10: Streamlines of the phase averaged velocity field in a reference frame moving with the mean convection velocity of the structures parallel to the wall for the co-flowing jet with (a,b,c) $H'_j/H_j = 0.5$, $U'_o/U_o = 0.36$, $f_R H_j/U_o = 0.49$ and (d,e,f) $H'_j/H_j = 0.18$, $U'_o/U_o = 0.56$, $f_R H_j/U_o = 0.28$ at $x/H_j = (a,d) 4$, $(b,e) 6$ and $(c,f) 8$.

Figure 11: Contours of $\tilde{w}_z H_j/U_o + (-\partial U/\partial y) H_j/U_o$ for the co-flowing jet with (a,b,c) $H'_j/H_j = 0.5$, $U'_o/U_o = 0.36$, $f_R H_j/U_o = 0.49$ and (d,e,f) $H'_j/H_j = 0.18$, $U'_o/U_o = 0.56$, $f_R H_j/U_o = 0.28$ at $x/H_j = (a,d) 4$, $(b,e) 6$ and $(c,f) 8$. **The cutoff level is ± 0.2 , the contour interval is 0.2.**

Figure 12: Typical distribution of $\tilde{w}_z H_j/U_o + (-\partial U/\partial y) H_j/U_o$ in (left) the flow with $H'_j/H_j = 0.5$ and $U'_o/U_o = 0.36$ and the flow with (right) $H'_j/H_j = 0.18$ and $U'_o/U_o = 0.56$, where the non-dimensional time delay $\tau^* = \tau U_o/H_j$. The cutoff level is ± 0.2 , the contour interval is 0.2.

Figure 13: Distributions of three components of the rapid pressure source terms from the phase averaged velocity field ($\tau^* = 0$), (a-b) $-2(\partial U/\partial y)(\partial \tilde{v}/\partial x)(H_j^3/U_o^2)$, (c-d) $-2(\partial V/\partial y)(\partial \tilde{v}/\partial y)(H_j^3/U_o^2)$, (e-f) $-2(\partial U/\partial x)(\partial \tilde{u}/\partial x)(H_j^3/U_o^2)$ for (left) the flow with $H'_j/H_j = 0.5$ and $U'_o/U_o = 0.36$ and the flow with (right) $H'_j/H_j = 0.18$ and $U'_o/U_o = 0.56$. The cutoff level is ± 0.01 , the contour interval is 0.05.

Figure 14: Distributions of one component of the rapid pressure source terms from the phase averaged velocity field, $-2(\partial U/\partial y)(\partial \tilde{v}/\partial x)(H_j^3/U_o^2)$, for (left) the flow with $H'_j/H_j = 0.5$ and $U'_o/U_o = 0.36$ and the flow with (right) $H'_j/H_j = 0.18$ and $U'_o/U_o = 0.56$. The cutoff level is ± 0.01 , the contour interval is 0.02.

Figure 15: Contribution of one component of the rapid pressure source terms from the phase averaged velocity field per unit mass to the wall pressure fluctuations at $x/H_j = 4$

, $(-1/4\pi r) * [-2(\partial U/\partial y)(\partial \tilde{v}/\partial x)(H_j^3/U_o^2)]$, for (*left*) the flow with $H'_j/H_j = 0.5$ and $U'_o/U_o = 0.36$ and the flow with (*right*) $H'_j/H_j = 0.18$ and $U'_o/U_o = 0.56$. The cutoff level is ± 0.001 , the contour interval is 0.004.

Figure 16: Comparison of the coefficient of (open symbols) the fluctuating wall pressure and (closed symbols) the phase averaged pressure with a reference at $x_R/H_j = 4$ in the flow with $\diamondsuit, \blacklozenge H'_j/H_j = 0.5$ and $U'_o/U_o = 0.36$ ($\dot{m}'/\dot{m} = 0.19$) and the flows with $H'_j/H_j = 0.18$ and $U'_o/U_o = \circlearrowleft, \bullet 0.56$ ($\dot{m}'/\dot{m} = 0.10$), $\square, \blacksquare 0.78$ ($\dot{m}'/\dot{m} = 0.14$) and $\triangle, \blacktriangle 0.91$ ($\dot{m}'/\dot{m} = 0.16$).

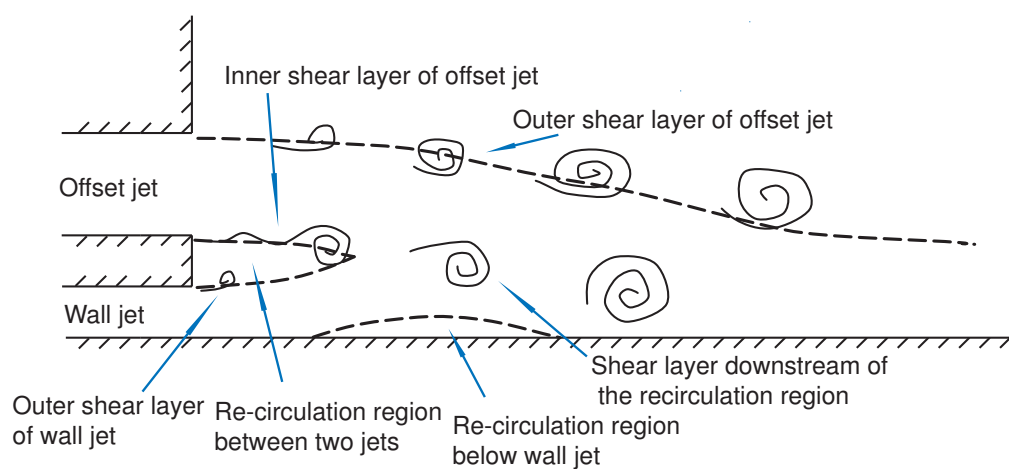


Figure 1:

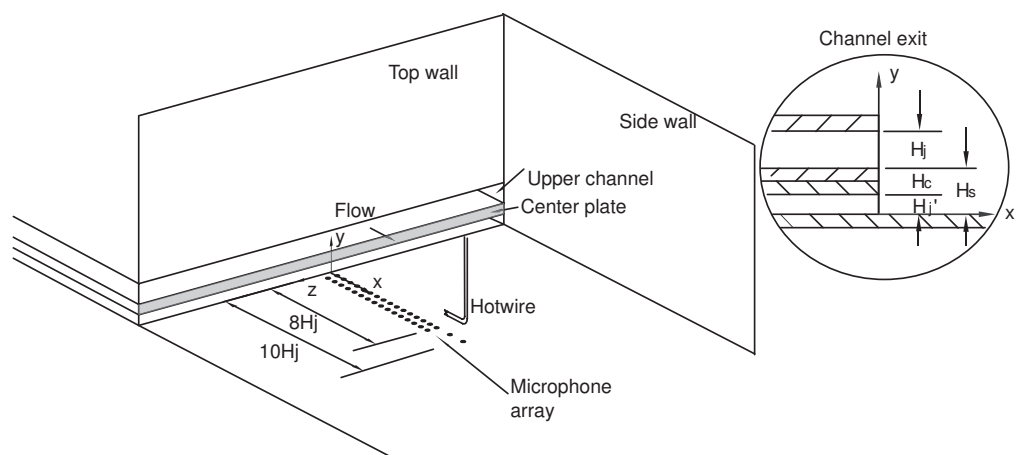


Figure 2:

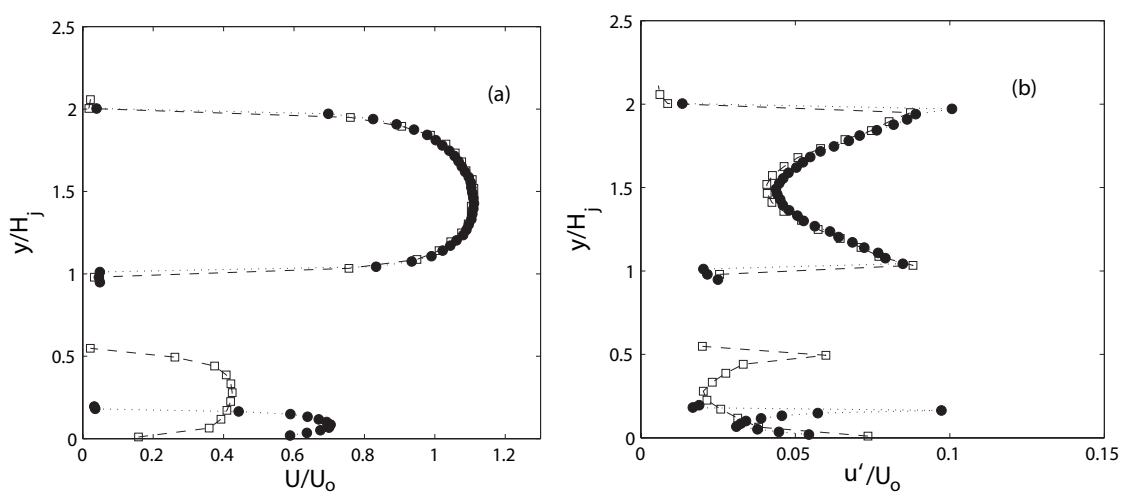


Figure 3:

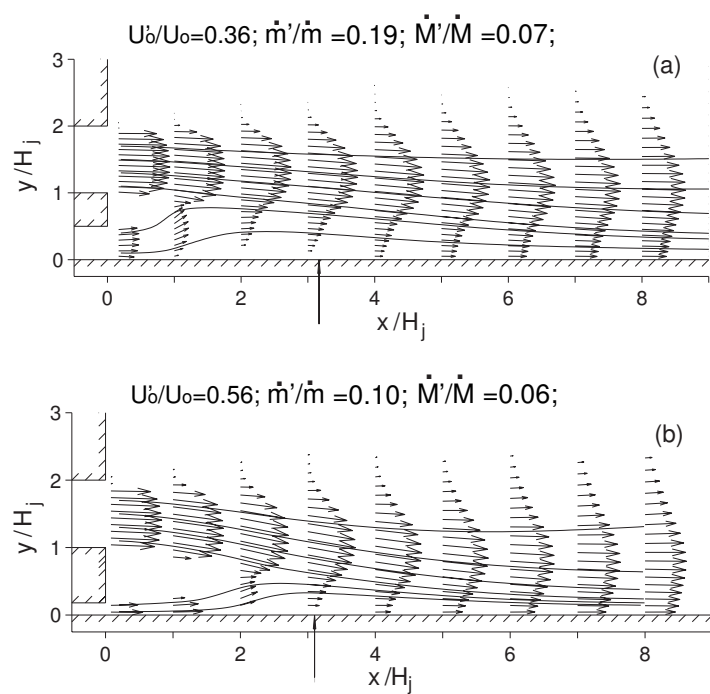


Figure 4:

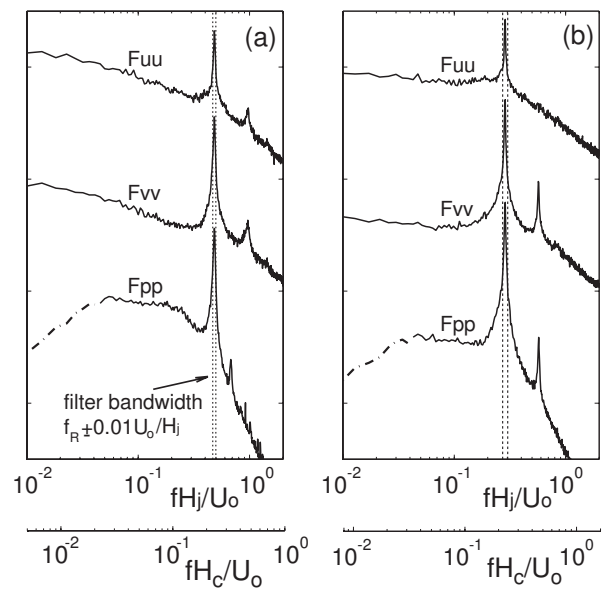


Figure 5:

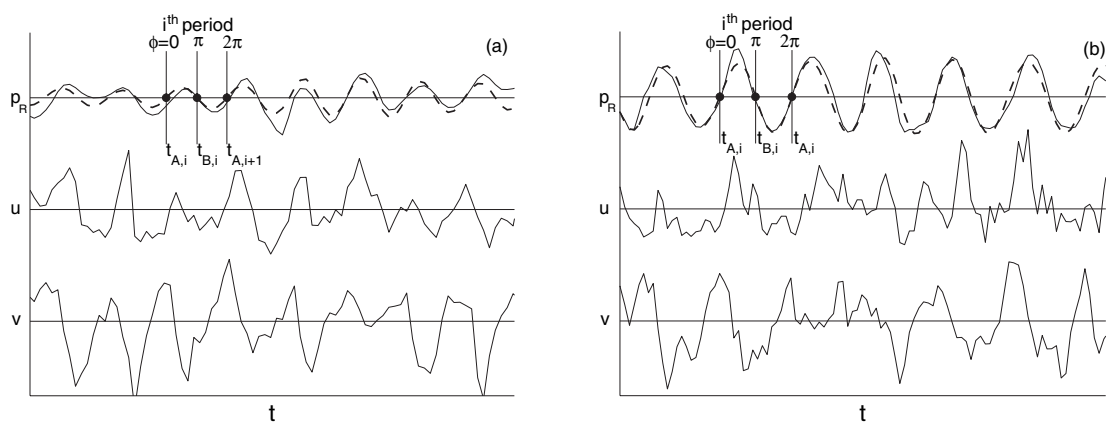


Figure 6:

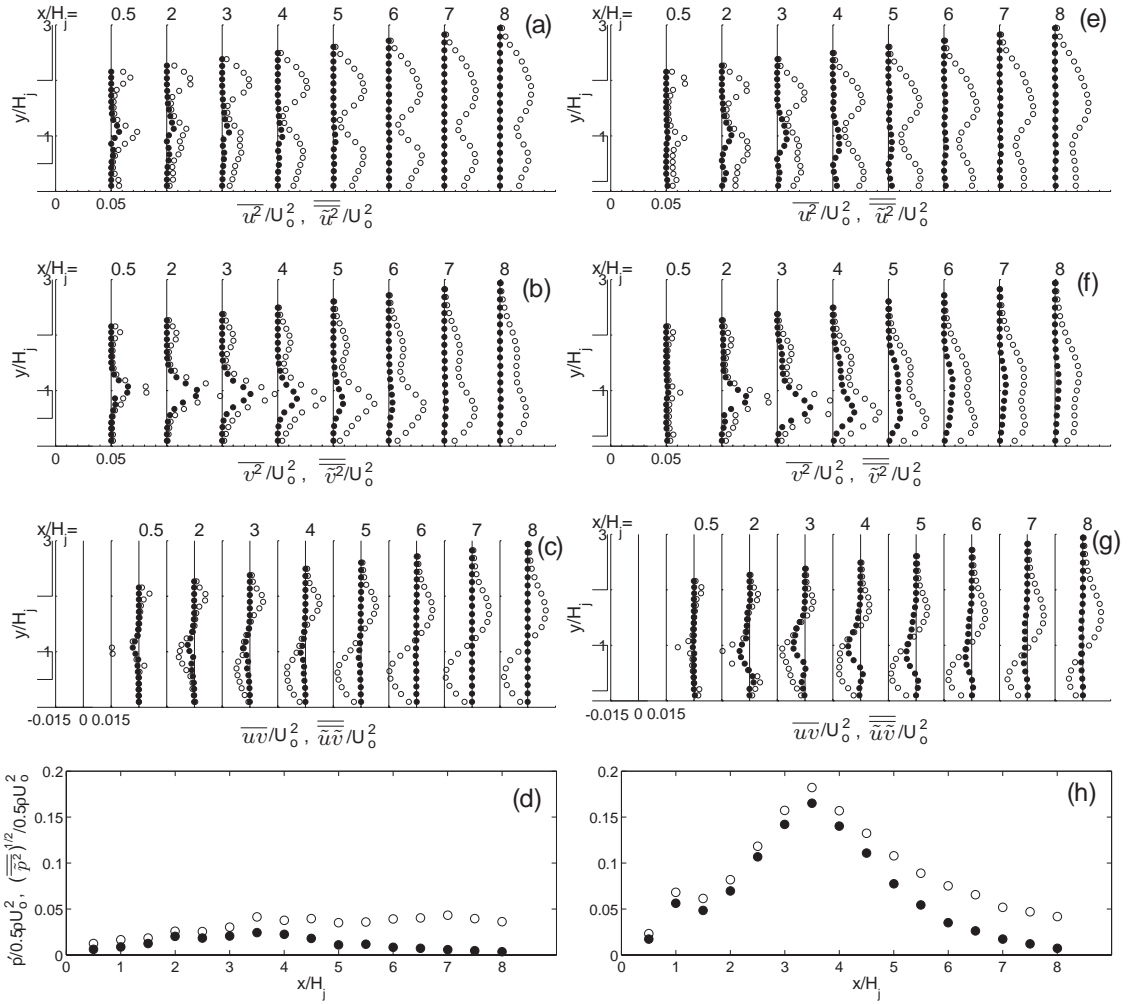


Figure 7:

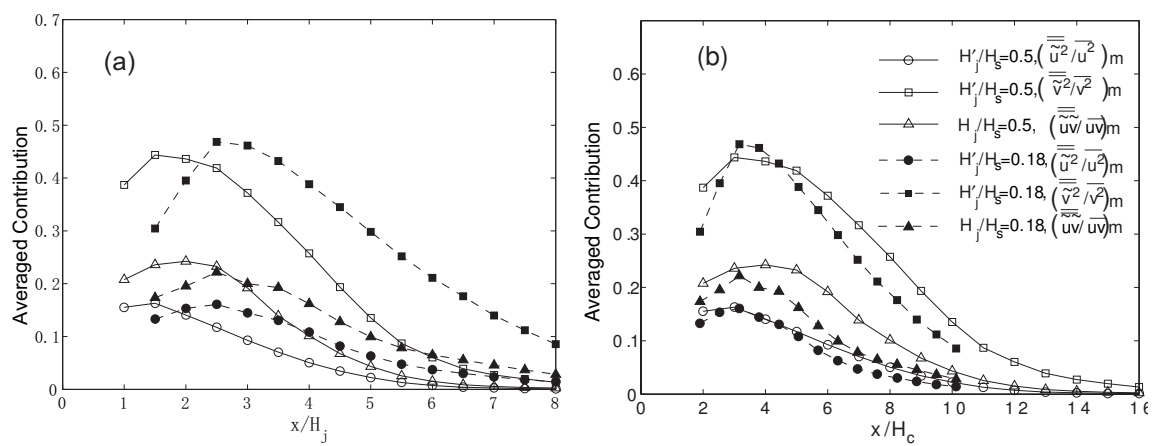


Figure 8:

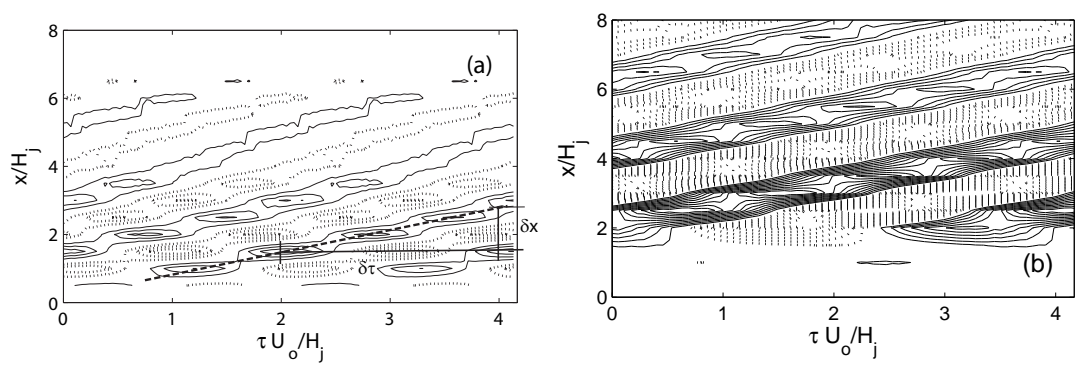


Figure 9:

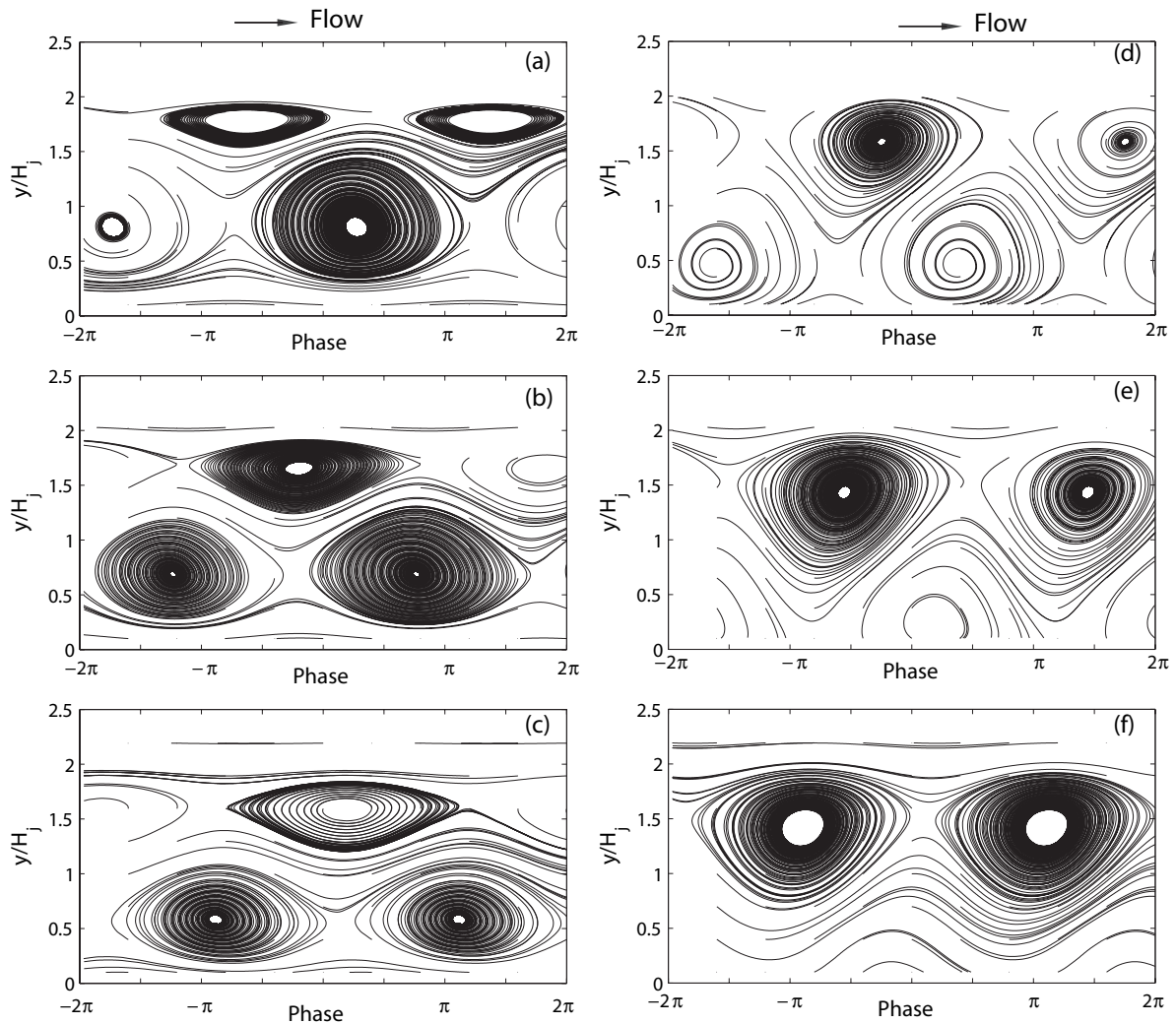


Figure 10:

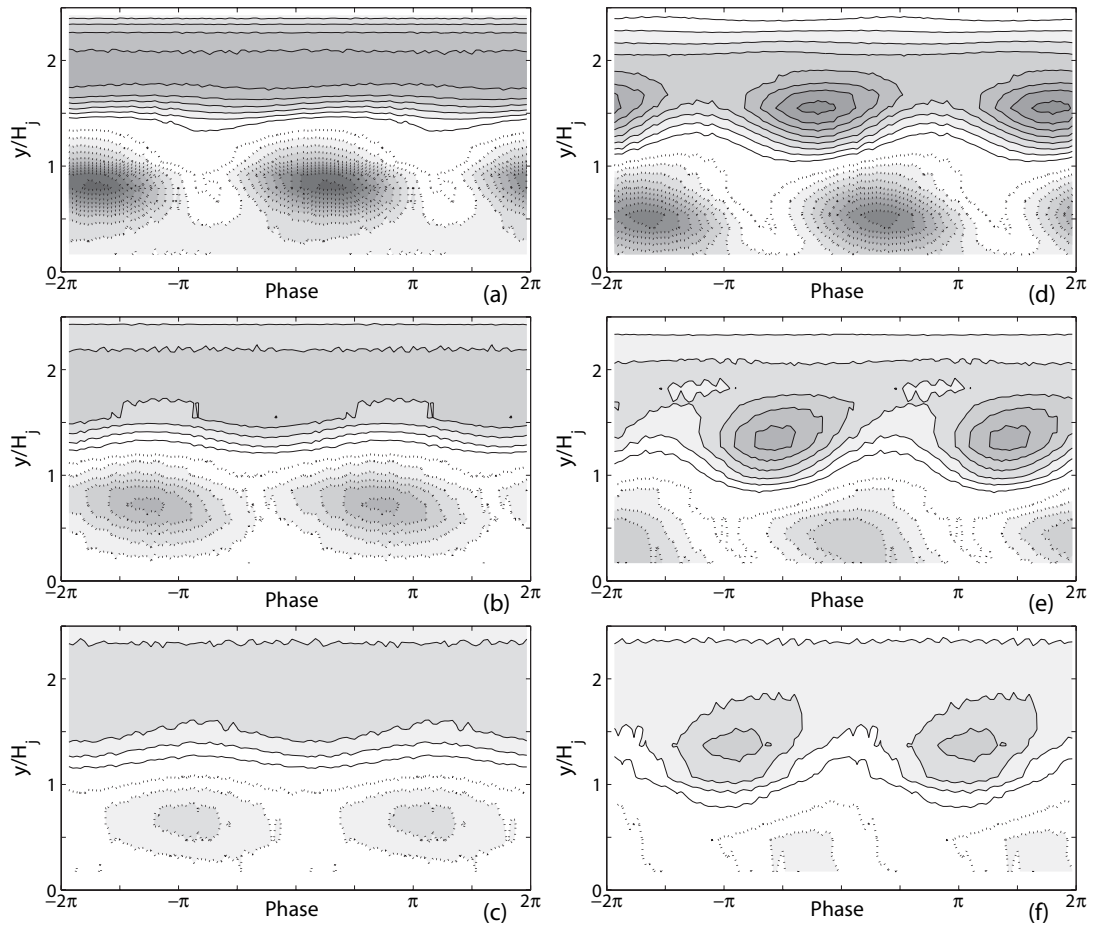


Figure 11:

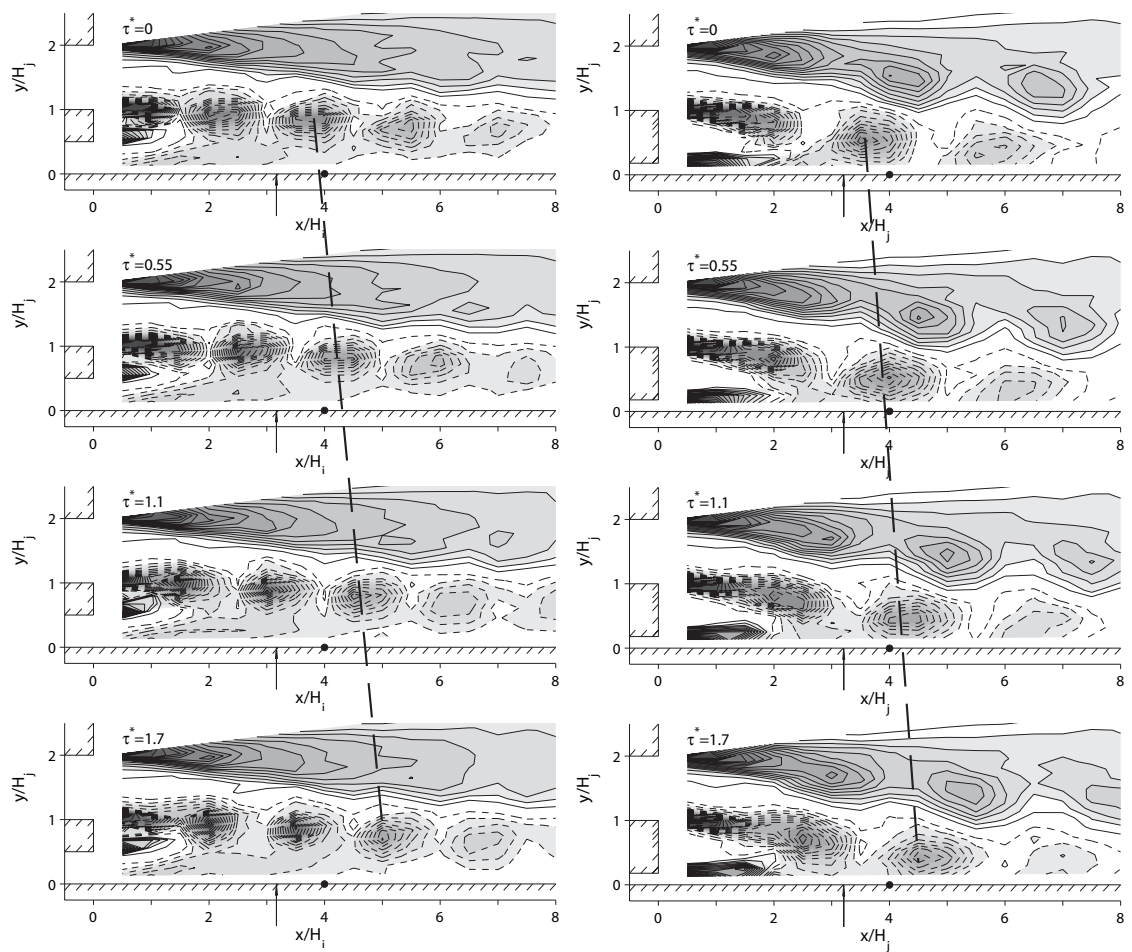


Figure 12:

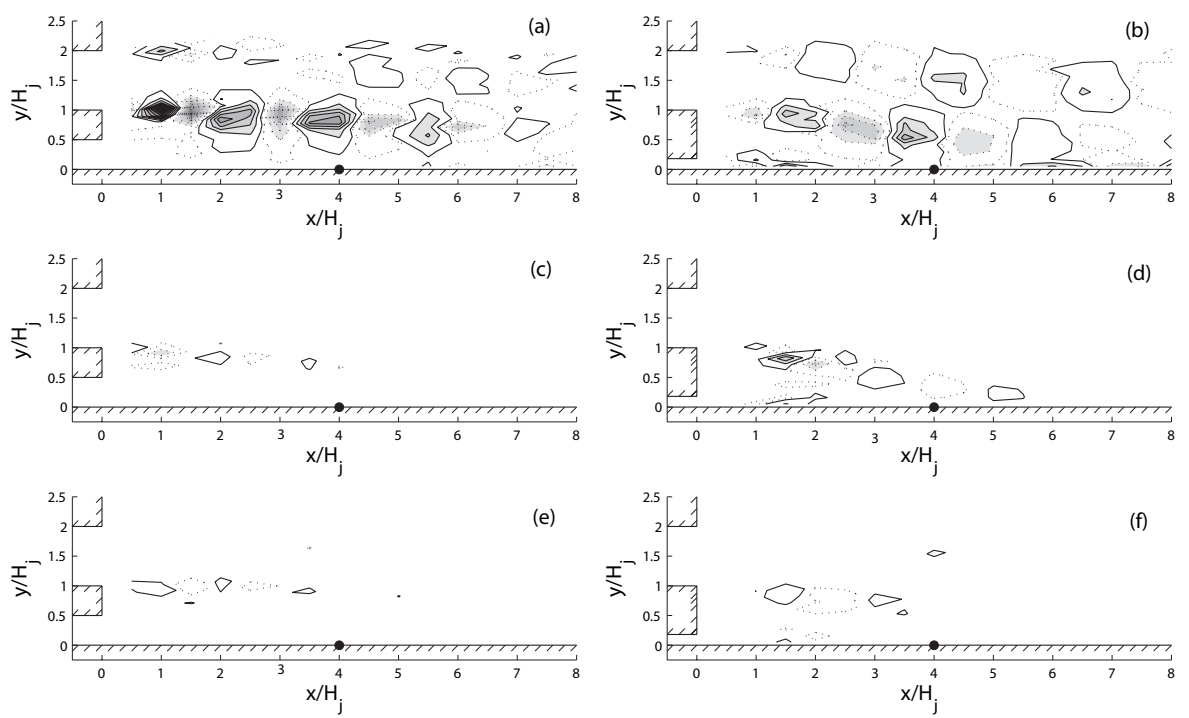


Figure 13:

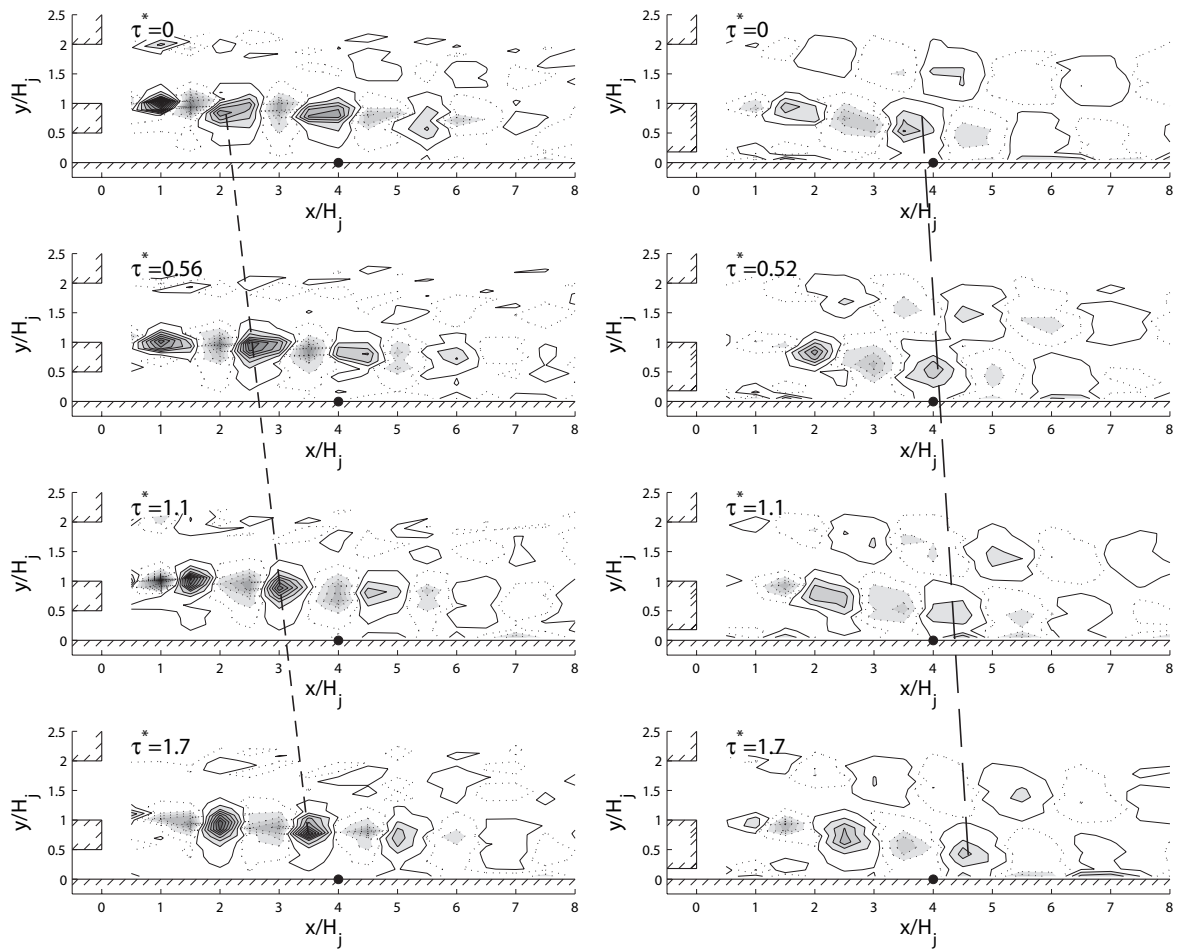


Figure 14:

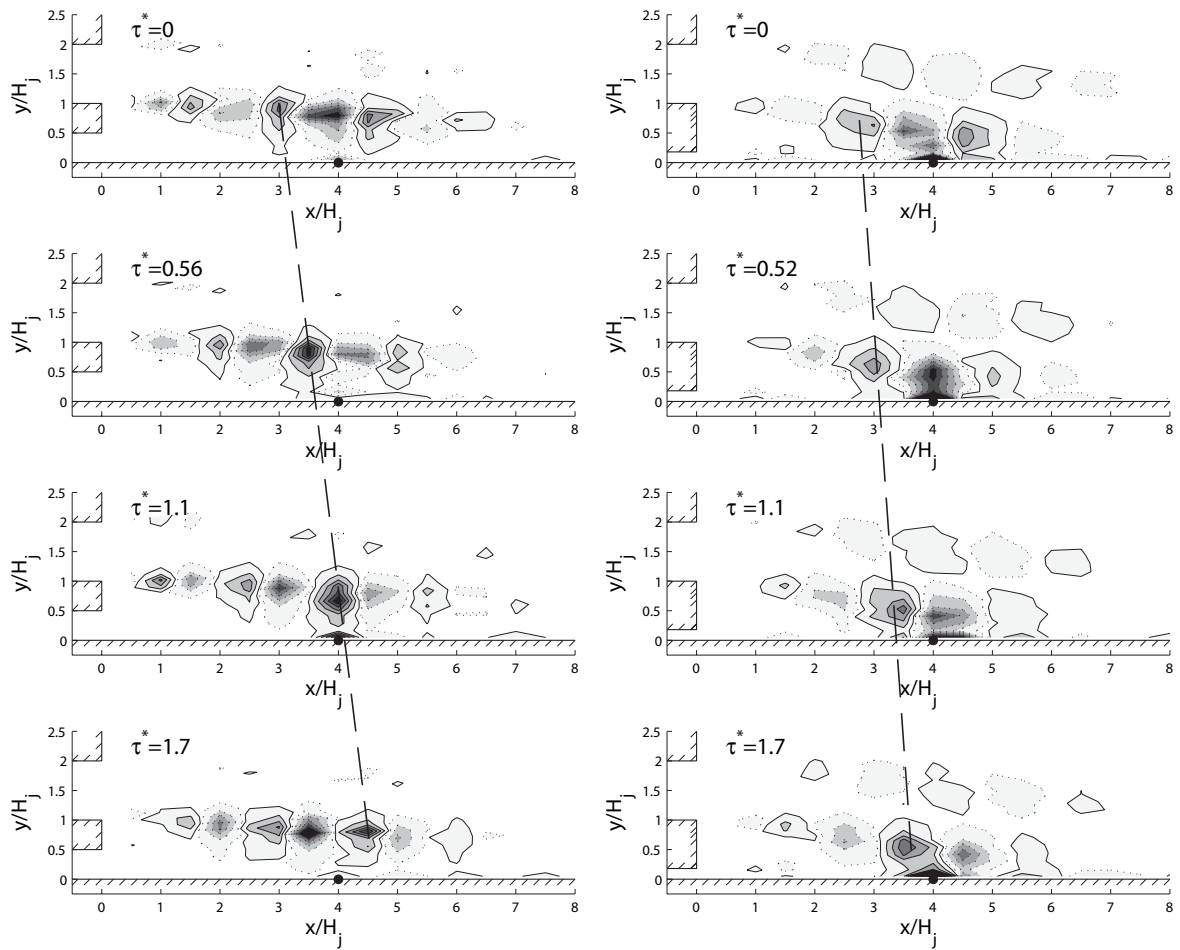


Figure 15:

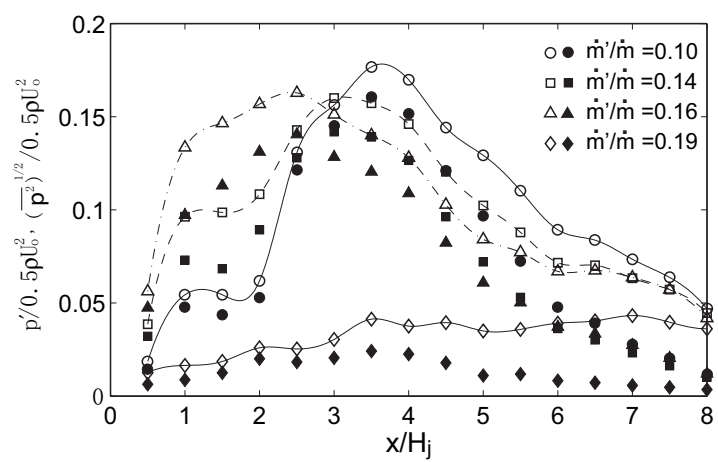


Figure 16: